Resource

Cell

A Mechanogenetic Toolkit for Interrogating Cell Signaling in Space and Time

Graphical Abstract

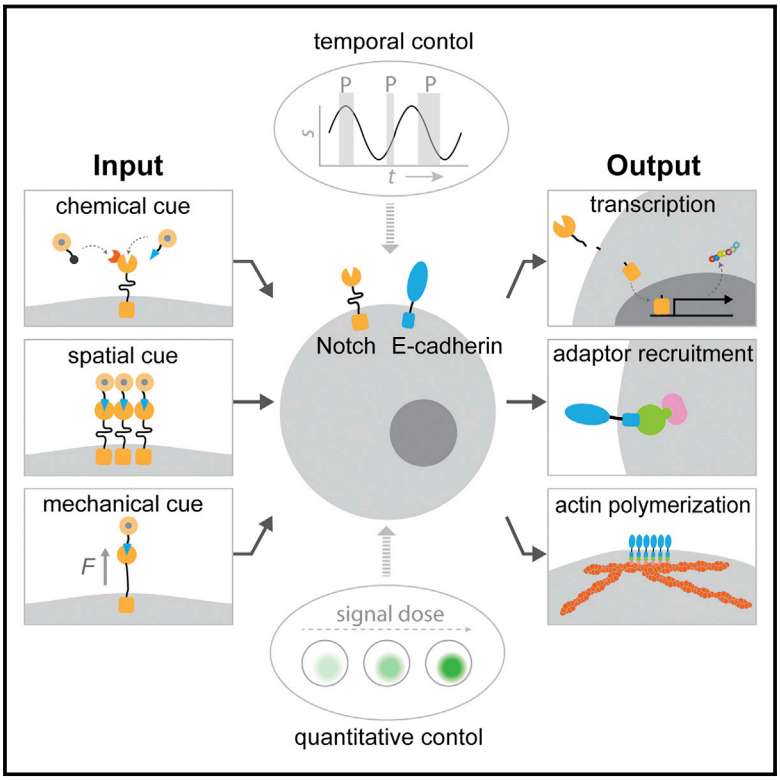

Authors

Daeha Seo, Kaden M. Southard, Ji-wook Kim, ..., Jinwoo Cheon, Zev J. Gartner, Young-wook Jun

Correspondence

zev.gartner@ucsf.edu (Z.J.G.), young-wook.jun@ucsf.edu (Y.J.)

In Brief

Mechanogenetics, a new approach that uses nanoparticles with imaging, localizing, and mechanically loading capabilities to activate targeted proteins with high spatiotemporal resolution, reveals how chemical, spatial, and mechanical cues cooperate to direct activation dynamics of Notch and E-cadherin receptors.

Highlights

- Development of a mechanogenetic single-cell perturbation approach
- Interrogation of the spatial, chemical, and mechanical responses of Notch receptors
- Identification of the roles of spatial and mechanical cues on E-cadherin signaling
- Spatiotemporal and quantitative control of single-cell transcription by nanoprobes

Seo et al., 2016, Cell *165*, 1–12
June 2, 2016
http://dx.doi.org/10.1016/j.cell.2016.04.045

CellPress

Please cite this article in press as: Seo et al., A Mechanogenetic Toolkit for Interrogating Cell Signaling in Space and Time, Cell (2016), http://dx.doi.org/10.1016/j.cell.2016.04.045

Cell

A Mechanogenetic Toolkit for Interrogating Cell Signaling in Space and Time

Daeha Seo,[1,2,3,4,11] Kaden M. Southard,[1,5,6,11] Ji-wook Kim,[7,8,9] Hyun Jung Lee,[1] Justin Farlow,[5,10] Jung-uk Lee,[7,8,9] David B. Litt,[2,3,4] Thomas Haas,[1] A. Paul Alivisatos,[2,3,4] Jinwoo Cheon,[7,8,9] Zev J. Gartner,[5,6,*] and Young-wook Jun[1,6,7,8,*]

[1]Department of Otolaryngology, University of California, San Francisco, San Francisco, CA 94115, USA
[2]Department of Chemistry and Department of Materials Sciences and Engineering, University of California, Berkeley, Berkeley, CA 94720, USA
[3]Materials Science Division, Lawrence Berkeley National Laboratory, Berkeley, CA 94720, USA
[4]Kavli Energy NanoScience Institute, University of California, Berkeley and Lawrence Berkeley National Laboratory, Berkeley, CA 94720, USA
[5]Department of Pharmaceutical Chemistry, University of California, San Francisco, San Francisco, CA 94158, USA
[6]Chemistry and Chemical Biology Graduate Program, University of California, San Francisco, San Francisco, CA 94158, USA
[7]Center for Nanomedicine, Institute for Basic Science (IBS), Seoul 03722, Republic of Korea
[8]Yonsei-IBS Institute, Yonsei University, Seoul 03722, Republic of Korea
[9]Department of Chemistry, Yonsei University, Seoul 03722, Republic of Korea
[10]Tetrad Graduate Program, University of California, San Francisco, San Francisco, CA 94158, USA
[11]Co-first author
*Correspondence: zev.gartner@ucsf.edu (Z.J.G.), young-wook.jun@ucsf.edu (Y.J.)
http://dx.doi.org/10.1016/j.cell.2016.04.045

SUMMARY

Tools capable of imaging and perturbing mechanical signaling pathways with fine spatiotemporal resolution have been elusive, despite their importance in diverse cellular processes. The challenge in developing a mechanogenetic toolkit (i.e., selective and quantitative activation of genetically encoded mechanoreceptors) stems from the fact that many mechanically activated processes are localized in space and time yet additionally require mechanical loading to become activated. To address this challenge, we synthesized magnetoplasmonic nanoparticles that can image, localize, and mechanically load targeted proteins with high spatiotemporal resolution. We demonstrate their utility by investigating the cell-surface activation of two mechanoreceptors: Notch and E-cadherin. By measuring cellular responses to a spectrum of spatial, chemical, temporal, and mechanical inputs at the single-molecule and single-cell levels, we reveal how spatial segregation and mechanical force cooperate to direct receptor activation dynamics. This generalizable technique can be used to control and understand diverse mechanosensitive processes in cell signaling.

INTRODUCTION

Mechanosensitive cell-surface receptors allow cells to sense the physical properties of the extracellular environment, including mechanical force resulting from cell-matrix and cell-cell interactions (Vogel and Sheetz, 2006). These receptors integrate mechanical, chemical (i.e., ligand-receptor interaction), spatial, and temporal cues (Iskratsch et al., 2014) to activate downstream signaling pathways implicated in development, homeostasis, and disease. Recent advances in imaging and force-sensing tools have extended our understanding of how mechanosensitive receptors transduce force from the cell exterior to the cytosol. However, little is known about how mechanosensitive receptors integrate mechanical signals with chemical, spatial, and temporal cues to differentially regulate downstream signaling pathways.

Single-cell perturbation techniques are required to understand how spatial and dynamic cues regulate downstream signaling pathways (Banghart et al., 2004; Deisseroth, 2011; Miesenböck, 2009; Toettcher et al., 2011). The key to this approach is the ability to quantitatively deliver a specific biochemical cue to any desired location and at any given time (Toettcher et al., 2011). Exemplary of this approach are optogenetic methods, where spatial and conformational control of light-sensitive proteins has provided systems-level mechanistic insight into a variety of neuroelectrical and biochemical signaling processes (Banghart et al., 2004; Deisseroth, 2011; Miesenböck, 2009; Toettcher et al., 2011). However, analogous methods do not exist for mechanosensitive signaling proteins. Microprobe-based force microscopy tools can deliver a specific force to purified biomolecules (Dufrêne et al., 2011; Neuman and Nagy, 2008), but, due to the large size and multivalent character of microprobes, these tools are not ideal for spatial control of individual membrane proteins in live cells because of their propensity to cluster upon binding (details are given in Results). Magnetic nanoparticles were previously used for controlling the subcellular distribution of proteins (Bharde et al., 2013; Cho et al., 2012; Etoc et al., 2013; Hoffmann et al., 2013; Mannix et al., 2008; Tseng et al., 2012) but have not been used for the mechanical loading of single biomolecules with controlled force. Therefore, new experimental tools are needed to probe the spatial, temporal, chemical, and mechanical regulation of mechanosensitive proteins in a single and integrated platform.

Please cite this article in press as: Seo et al., A Mechanogenetic Toolkit for Interrogating Cell Signaling in Space and Time, Cell (2016), http://dx.doi.org/10.1016/j.cell.2016.04.045

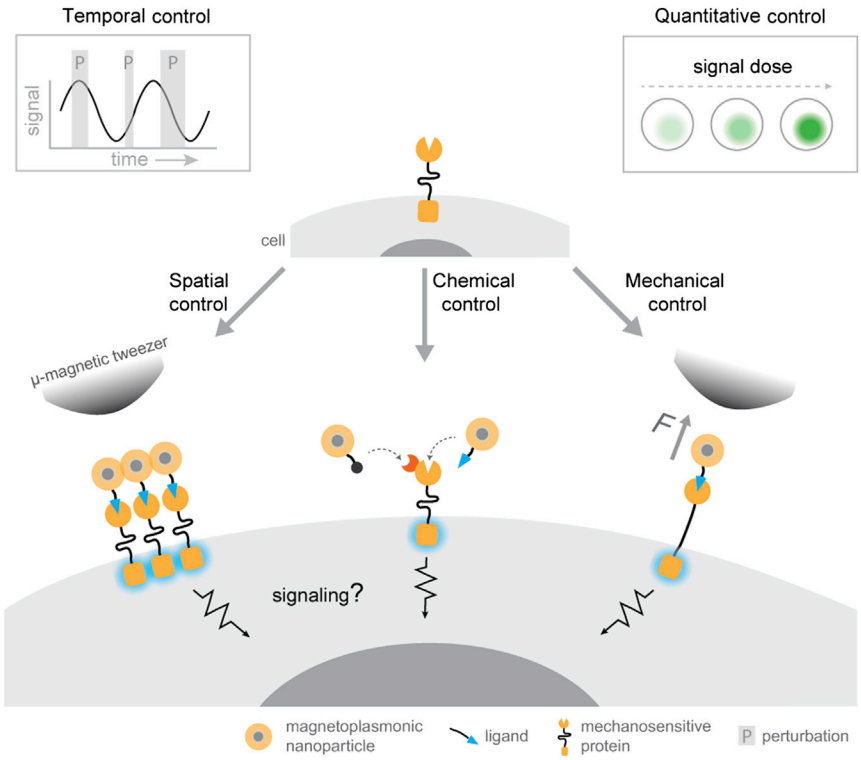

Figure 1. A Magnetoplasmonic Nanoprobe System for Spatial, Chemical, and Mechanical Control of Cell Signaling

When targeted to mechanosensitive proteins expressed at the cell surface, the magnetoplasmonic nanoparticle (MPN) probes can deliver a variety of controlled perturbation: Chemical control is derived via ligand-receptor interactions or the use of genetically encoded targeting domains (e.g. SNAP). Spatial control is achieved through application of a focused magnetic field gradient to defined subcellular locations and subsequent nanoparticle relocalization. Additionally, by increasing the magnetic field gradient by moving the tweezer toward the cell surface, nanoprobes can mechanically load targeted proteins, inducing conformational changes (Mechanical control). Each independent MPN-driven cue can be applied at any given time (Temporal control) and with any desired dose (Quantity control).

To address this unmet need, we developed a platform nanotechnology tool based on monovalent targeted magnetoplasmonic nanoparticles (MPNs) capable of localizing, visualizing, and mechanically activating mechanosensitive proteins at the single-cell or -molecule level. To demonstrate the utility of these modular nanoprobes, we investigated two important membrane proteins involved in cell-cell communication—Notch and E-cadherin. We first show that MPNs target mechanosensitive proteins with monovalent and stoichiometric ligand-receptor binding, programmed spatial reorganization, and targeted delivery of mechanical signals while reporting on these processes with single-molecule and single-cell resolution (Figure 1). We reveal that mechanical force is sufficient to activate the Notch receptor independent of receptor clustering and ligand binding, and we reveal the differential role of E-cadherin clustering and mechanical loading in the nucleation and stabilization of actin filaments.

RESULTS

Synthesis of Multifunctional MPN Probes

We synthesized colloidal MPNs via sequential growth of a magnetic Zn-doped ferrite ($Zn_{0.4}Fe_{2.6}O_4$) core, a dielectric silica layer, and a plasmonic gold shell (Figure 2A; Figure S1), where the magnetic core and the plasmonic shell serve as the force-generating and the imaging components, respectively. We chose a Zn-doped ferrite core (Figure S1) and a plasmonic Au shell geometry to maximize the magnetic and optical properties of the nanoprobe (Jang et al., 2009; Wang et al., 2007). The integrated system allows piconewton force delivery and robust single-molecule imaging signals while maintaining a small overall size. The MPNs were highly monodisperse in diameter (mean = 50 nm, σ = 8%) and thus provided optically monodisperse scattering signals (Figures 2A and S1). The size of each component and the total size of the nanoparticles were independently controllable, providing additional capabilities to tune the force-generating and optical properties (Wang et al., 2007) (Figure S1).

Nanoprobe-Mediated Spatial Reorganization and Force-Induced Structural Changes of Biomolecules In Vitro

To confirm that MPNs were capable of mechanically controlling both the spatial localization and conformation of targeted biomolecules, we evaluated their properties in two in vitro model systems. First, we tested the capacity of benzyl guanine (BG)-modified MPNs (BG-MPN; details are given later) to control the spatial organization of a model SNAP-tagged protein without affecting their diffusion on a supported lipid bilayer (SLB) (Farlow et al., 2013). We monitored the lateral diffusion of the MPN-labeled proteins by total internal reflection dark-field (TIR-DF) microscopy and generated a focused magnetic field gradient across the membrane using a piezo-controlled micromagnetic tweezer with a round-tip end (tip radius: 5.1 μm) oriented vertically to the bilayer. The field gradient in the proximity of the particles was tuned by changing the tip-to-bilayer distance (d) (Figure 2C). At $d \leq 10$ μm, the MPN efficiently drives the directional migration of labeled SNAP-tag proteins toward the targeted position and eventually traps the proteins in a desired location (Movie S1). Investigation of the effective length for migration (i.e., diameter of the concentrated circle upon saturation) (Figures 2D and 2E) as a function of d and the field application time (t) revealed an optimal tweezer configuration suitable for single-cell manipulation. We found that d = 2–5 μm allowed rapid attraction of all SNAP-tag proteins with 4-μm resolution (i.e., smallest diameter of the concentrated

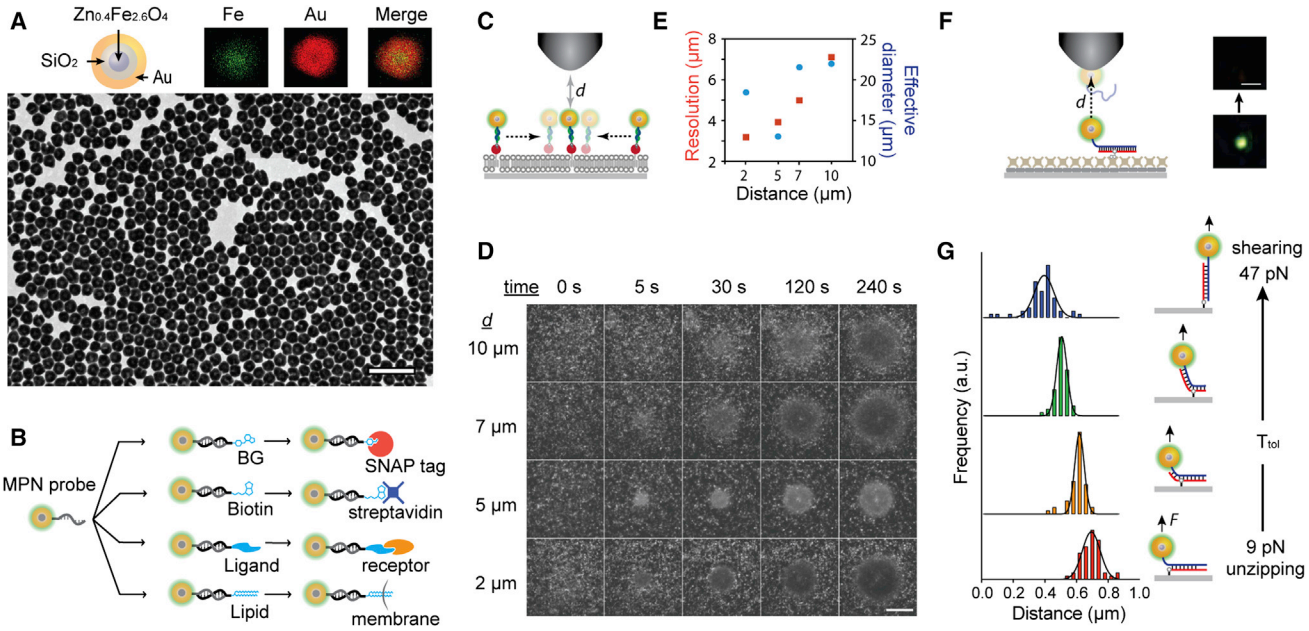

Figure 2. Imaging, Targeting, and Force-Generating Capabilities of the MPNs

(A) Characterization of MPNs. Transmission electron microscope (TEM) images and elemental mapping revealed uniform size dispersity (50 ± 4 nm) and composition. Scale bar, 200 nm.

(B) Modular functionalization of MPNs.

(C–E) Spatial control of SNAP-tag protein diffusion across a supported lipid bilayer (SLB) by MPNs. (C) Experimental scheme. We directed a micromagnetic tweezer vertically toward the lipid bilayer while changing the tip-to-membrane distance (d) between the tweezer and the SLB. (D) Representative images of concentrated nanoparticle assemblies. Scale bar, 10 μm. (E) The lateral resolution and effective length of concentration as a function of d.

(F and G) In vitro characterization of force delivery by MPNs. (F) Experimental scheme and dark-field images of MPN-induced single-molecule rupture of a dsDNA. Scale bar, 2 μm. (G) The most probable rupture distances of DNAs with various immobilization geometries.

circle) and 10–20 μm effective length. Note that relocalization of the proteins was induced by force-induced active transport (Etoc et al., 2013; Hoffmann et al., 2013; Mannix et al., 2008; Tseng et al., 2012) rather than by passive diffusion followed by the trapping of proteins, as in optogenetic methods (Levskaya et al., 2009). This property of MPNs is advantageous for directing the reorganization of confined or slowly diffusing membrane proteins such as Notch and E-cadherin receptors (Farlow et al., 2013).

We also examined the capacity of the MPNs to exert a prescribed force to a targeted biomolecule tethered to the MPN. We used force-induced rupture of a double-stranded DNA (dsDNA) by the MPN because of its well-defined tension tolerance (T_{tol}) at a fixed loading rate and their demonstrated utility to sense force exerted by mechanical receptors (Cocco et al., 2001; Ho et al., 2009; Wang and Ha, 2013). We monovalently conjugated MPNs to dsDNA in an unzipping rupture geometry with T_{tol} of 9 pN (Figure S2) (Cocco et al., 2001; Ho et al., 2009; Wang and Ha, 2013). The 5′-thiolated end of one strand was bound to the nanoparticle, while a 3′-biotin functional group on the opposite strand was tethered to a streptavidin-coated coverslip. Force was applied by gradually decreasing d with a step size of 20 nm (approach rate, 100 nm/s) above a target particle under TIR-DF microscopy. Particle detachment at increased force indicated force-induced rupture of dsDNA (Figure 2F; Figure S3). Statistical analysis of the rupture events provided the most probable rupture distance at d = 0.7 μm. Repeating these experiments using a panel of dsDNA having different T_{tol} (Cocco et al., 2001; Mosayebi et al., 2015; Wang and Ha, 2013) revealed a gradual decrease in rupture distance with increasing T_{tol} (Figure 2G).

Modular Targeting and Valency of MPN Probes

MPNs require facile and modular bio-conjugation to enable their application to diverse biological systems. We introduced targeting functionality to MPNs by first conjugating them to a 5′-thiol-functionalized oligonucleotide. We chose an oligonucleotide as a tether because of its ease of synthesis, defined valency, and facile targeting through hybridization or direct covalent modification (Figure 2B) (Farlow et al., 2013; Weber et al., 2014). For example, we synthesized monovalent MPNs bearing either a BG- or biotin-functional group (Figure S3), which were used to label various SNAP-tagged or streptavidin-linked targets, respectively, with high specificity (Figure S3). The same BG-MPNs could be targeted using protein ligands expressed as fusions to the SNAP-tag (e.g., delta-like ligand-1; Dll1) (Figure S4). The valency of MPNs could be controlled easily by changing reaction stoichiometry between the MPNs and thiolated oligonucleotides (Figure S3).

To investigate the specificity of these nanoprobes to a single targeted cell-surface receptor, we generated a U2OS stable cell line expressing a recombinant human Notch 1 protein

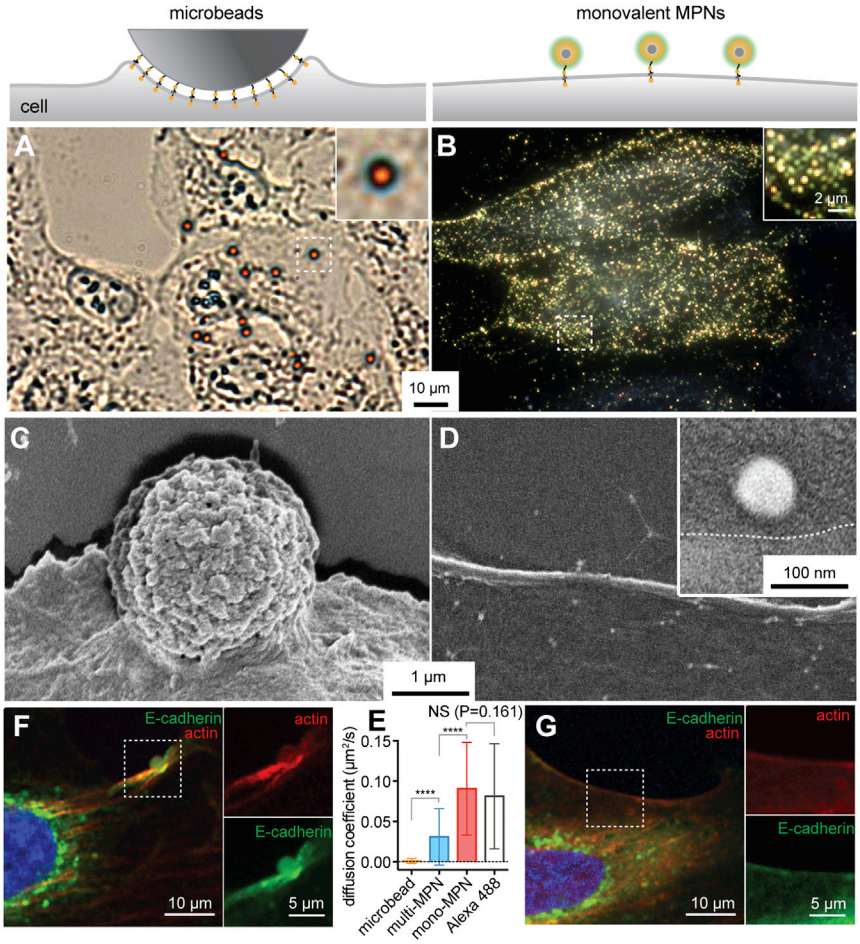

Figure 3. Effect of MPNs and Microbeads on Cell Architecture and Signaling after Probe Labeling

(A–F) Optical imaging of (A) microbead- or (B) MPN-labeled U2OS cells expressing SNAP-hN1-mCherry receptors. MPN probes show dense labeling. Scanning electron microscopy images of (C) microbead- or (D) MPN-labeled cells expressing Notch. Inset image show a 10× magnification on a single MPN. The cell edge is outlined in white. (E) Diffusion of Notch receptors labeled with magnetic microbeads or MPN probes. (F) Confocal microscopy of U2OS cells expressing E-cadherin, after labeling with (F) a microbead or (G) MPNs in the absence of any magnetic perturbation. Error bars indicate SE. ****$p < 0.0001$. NS, not significant.

fused with SNAP- and mCherry-tags at its N and C termini (SNAP-hN1-mCherry) (Farlow et al., 2013), respectively. Bright scattering spots from the cells were observed only for the cells expressing SNAP-hN1-mCherry (Figure S4), indicating specific Notch targeting via BG/SNAP chemistry. Specific targeting of Notch receptors via ligand-receptor chemistry was also possible by treating the cells with Dll1-functionalized MPNs (Figure S4). We also targeted a different cell-surface receptor, E-cadherin, using the same BG-SNAP targeting chemistry. (Figure S4).

MPNs versus Microbeads for Cell Applications

The activation of mechanosensitive proteins is regulated by ligand binding, oligomerization, spatial organization, mechanical loading, and processing by a number of downstream proteins. To discriminate between these modes of regulation, the probe must not change the properties of targeted molecules or their mechanical microenvironment in the absence of an externally applied stimulus (Dufrêne et al., 2011).

To test whether our nanoprobe system provides improved capabilities in this regard when compared to more traditional microbead-based tools, we labeled U2OS cells expressing SNAP-hN1-mCherry with BG-MPNs or with microbeads (M280 Dynabeads, ThermoFisher) via identical procedures. We then directly compared the two tools with respect to their ability to specifically and efficiently label target proteins, and their tendency to perturb the mechanical microenvironment in the absence of an external magnetic field. Microbeads and MPNs showed dramatic differences in all aspects tested. Microbead attachment was sparse (typically, zero to five per cell) (Figure 3A). Moreover, we observed significant perturbation of cell-surface structure by microbead labeling, as shown by scanning electron microscopy (Figures 3C and S4). Additionally, microbead labeling significantly disrupted receptor diffusion and downstream signaling activity without the application of external magnetic fields. For example, Notch receptors were completely immobilized after microbead labeling (diffusion coefficient, $<5 \times 10^{-4}$ $\mu m^2/s$) (Figure 3E). Similarly, E-cadherin clustering and F-actin polymerization (Figure 3F) were also observed upon microbead labeling, even without the application of an external magnetic field. In contrast, monovalent MPNs yielded dense Notch receptor labeling (10^3–10^5 particles per cell, depending on the protein expression level) (Figure 3B) and minimal perturbation of cell-surface structure in the absence of an applied magnetic field (Figure 3D). We could not detect any signature of alterations in Notch receptor diffusion (Figure 3E) or E-cadherin signal activation (Figure 3G; Figure S4) by MPN labeling, illustrating the superior properties of MPNs as a perturbation tool over traditional microbeads.

Subcellular Localization of Targeted Proteins at Prescribed Locations, Quantities, and Times

Next, we tested the capability of the MPNs to drive the physical localization of receptors on live cells. After labeling cells expressing SNAP-hN1-mCherry or SNAP-Ecad-mEmerald receptors with BG-MPNs, we set the micromagnetic tweezer to a weak-force exertion mode, in which the tweezer was placed 2 or 5 μm above a target subcellular location so as to affect the

localization of the labeled receptors without activation. We monitored changes in nanoprobe and targeted protein distribution by both reflective dark-field and fluorescence microscopy, respectively. Immediate relocalization of the nanoprobe to a 5-μm diameter region was observed (Movie S2). Time traces of the MPN and fluorescence intensities at the targeted area showed gradual increase followed by saturation (Figure S5). For example, statistical analyses ($n \geq 10$) of the saturated MPN density and SNAP-hN1-mCherry signals showed average 3.7-fold and 3.6-fold increases compared to the initial values, respectively (Figure S5). Spatially and quantitatively controlled protein relocalization to desired subcellular locations was easily achieved by adjusting tweezer position and application time (Figures 4A–4C; Figure S5). The concentration of particles by the magnetic field was reversible by simply removing the tweezer, without any signature of residual particle aggregation (Movie S3). The capability of the MPNs to spatially segregate target proteins (i.e., Notch or E-cadherin) was useful not only for mimicking spatial segregation of mechanosensitive proteins at cell-cell interfaces observed in vivo but also for investigating the impact of spatial segregation on downstream signaling events.

Force Generation Is Sufficient to Activate Notch Independent of Spatial Reorganization or Ligand Identity

Notch is a key juxtracrine signaling molecule involved in numerous physiological, developmental, and pathological processes. Initiated by ligand-receptor binding between neighboring cells, Notch receptors undergo dynamic spatial, chemical, mechanical, and structural changes, including receptor segregation, receptor clustering, force generation, and receptor proteolysis. These events culminate in the release of the Notch intracellular domain, which traffics to the nucleus to affect gene transcription (Kopan and Ilagan, 2009; Louvi and Artavanis-Tsakonas, 2006). The relative involvement of spatial, chemical, and mechanical cues during this complex process remained to be resolved.

Most studies have emphasized the importance of force-induced unfolding within the negative regulatory region (NRR) domain of Notch, which exposes the S2 cleavage site to metalloprotease activity, as a key step in activating downstream cell signaling (Gordon et al., 2007; Stephenson and Avis, 2012). However, conflicting reports also implicate receptor clustering, oligomerization, and allosteric structural changes of the NRR domain due to ligand-receptor interaction as key to activation (Kopan and Ilagan, 2009). Very recently, Gordon and colleagues combined microbead-based force microscopy and a synthetic ligand-receptor system to address the relative importance of ligand-induced allosteric changes relative to mechanical loading during Notch receptor activation (Gordon et al., 2015). Their results conclusively demonstrated that mechanical loading is sufficient to activate the receptor in the absence of native ligand. However, because large and multivalent microbeads were used in this study, which can cluster and immobilize receptors, the relative role of receptor oligomerization and spatial reorganization during force-mediated receptor activation could not be resolved.

To identify whether receptor oligomerization or clustering are also necessary for force-mediated activation of Notch, we utilized the unique 1:1 binding of MPNs to single Notch receptors to control their position, oligomerization, and mechanical loading at the cell surface. First, we examined the mechanical response of individual Notch receptors on live cells with single-molecule resolution. Because MPNs are monovalent and can be directly imaged in the dark field, we could be certain that any force delivered to an MPN was relayed to a single ligated Notch receptor. We applied either a weak force (d = 2 μm, 1 pN per particle; Figure S5) or a strong force (d = 0.7 μm, 9 pN per particle; Figure 2G) to a randomly chosen single particle diffusing on a sparsely labeled cell membrane. At 1 pN pulling force, the particle was rapidly trapped at the targeted location but did not dissociate even with prolonged treatment over 10 min (Figure 4D). At 9 pN pulling force, in contrast, we observed detachment of particles from the cell surface within a few seconds (Figure 4D). These data suggest that mechanical loading of single Notch receptors, above a critical force, is sufficient to initiate rapid Notch extracellular domain (NECD) shedding, consistent with recent in vitro single-molecule force microscopy studies (Gordon et al., 2015). To test whether receptor aggregation was also sufficient for NECD dissociation, we performed similar experiments on densely labeled cells. We directed Notch receptors to specific subcellular locations under weak mechanical loading insufficient to activate single receptors. Neither detachment of particles (Figure S5) nor decrease in mCherry fluorescence intensities were seen, even after prolonged treatment (Figure 4E). However, an increase in mechanical loading from 1 pN to 9 pN initiated a significant decrease of both particle scattering (Figure S5) and mCherry fluorescence (Figures 4E and 4F; Movie S2) intensities relative to initial values ($\Delta I/I_o = 48 \pm 23\%$). These observations are consistent with the detachment of the nanoprobes and loss of Notch proteins from the targeted area, respectively. We interpreted these observations to be a consequence of the force-induced unfolding of the NRR domain followed by subsequent S2 cleavage of the Notch construct (Gordon et al., 2007). To confirm this, we performed an identical experiment in the presence of an inhibitor of S2 cleavage (TAPI-2) and/or a γ-secretase-mediated S3 cleavage (DAPT). When TAPI-2 was included, negligible changes in mCherry fluorescence signals of the target area ($\Delta I/I_o < 4\%$, $p = 0.078$) were observed (Figures 4E and 4F), ruling out the possibility of nonspecific particle detachment or membrane rupture. When only DAPT was added, we observed results similar to those for the non-inhibited conditions (Figure 4F) ($\Delta I/I_o = 39 \pm 24\%$), suggesting that decrease in mCherry fluorescence intensity required S2 cleavage and likely was followed by diffusion of the S2-cleaved products away from the targeted location.

To confirm that the force-dependent shedding of the NECD also activated downstream signaling, we used a UAS-Gal4 reporter system where Notch signal activation triggers transcription and nuclear localization of mCherry reporter (Figure S6). After labeling cells with the MPNs, we targeted cells in either the weak- or strong-force modes for 15 min and monitored nuclear mCherry fluorescence. Consistent with the aforementioned results from the S2 cleavage experiments, only the cells treated with the strong-force mode showed bright nuclear fluorescence

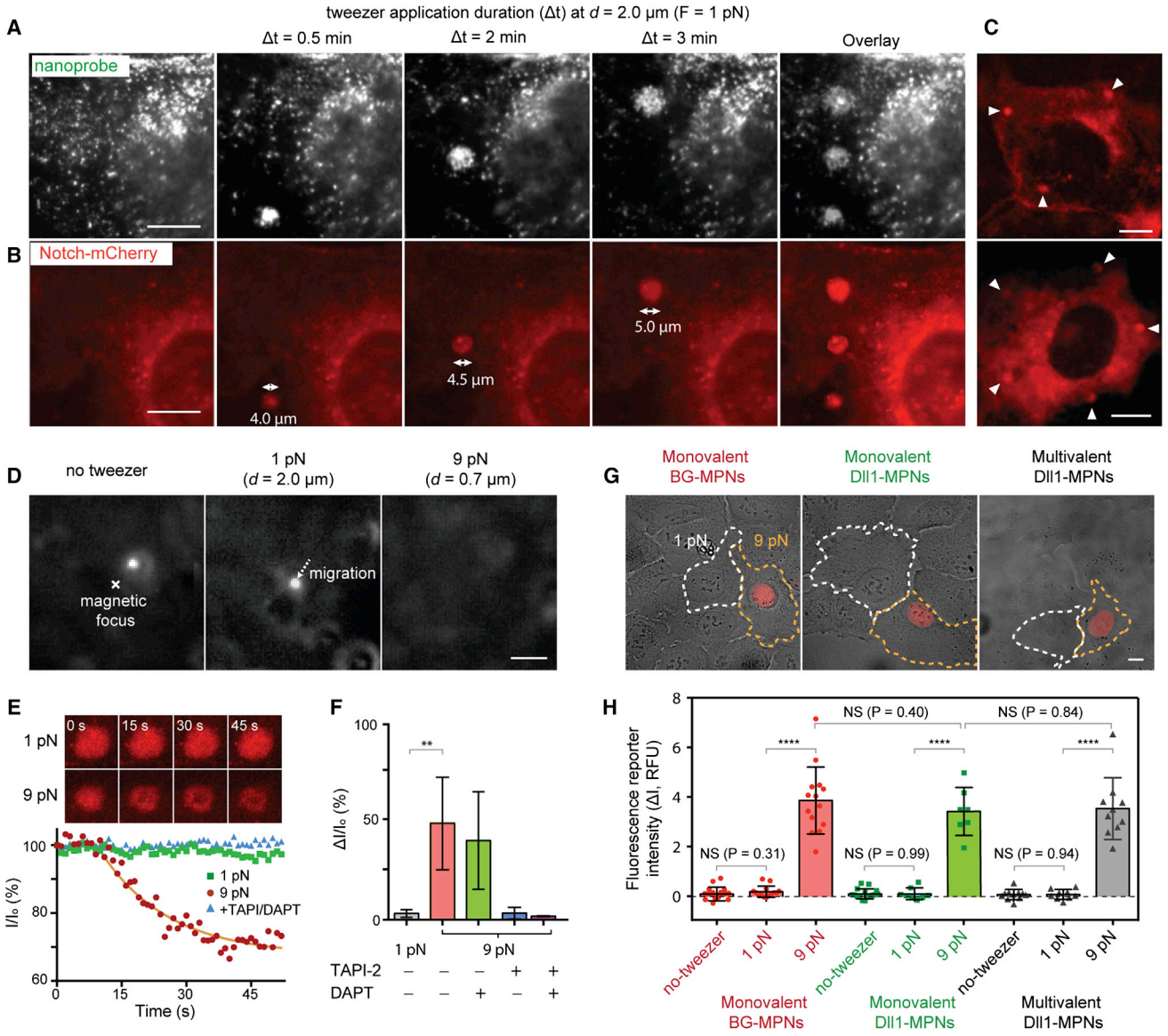

Figure 4. Responses of Notch Receptors to Spatial, Mechanical, and Chemical Perturbation with MPNs

(A–C) Spatial control of MPN-labeled Notch receptors expressed in U2OS cells. Representative images of spatially segregated (A) MPNs and (B) Notch in a cell. (C) Other representative overlay images. Scale bars, 10 μm.

(D–F) Force response of Notch receptors at the cell surface. (D) Dark-field images of MPN-labeled Notch after weak-force (1 pN at d = 2.0 μm) or strong-force (9 pN at d = 0.7 μm) application. No particle detachment was seen under the weak force, while immediate detachment of the particle was observed with strong force. Scale bar, 2 μm. (E) Time traces of mCherry fluorescence signal of pre-concentrated Notch after weak- or strong-force application. (F) Statistical analysis of mCherry fluorescence signal after force application with or without inhibition. Error bars indicate SE.

(G and H) Effects of receptor segregation, mechanical force, and ligand-receptor interaction on Notch signal activation. (G) Optical imaging of UAS-Gal4 cells after varying stimulation with respect to targeting chemistry (BG/SNAP versus Dll1-Notch), particle valency (monovalency versus crosslinkable multivalency), and force magnitude (strong versus weak). Scale bar, 10 μm. (H) Statistical analysis of Notch activity with multiple replicates. Error bars indicate SE.

**p < 0.01; ****p < 0.0001; NS, not significant.

signals, while the cells treated with the weak-force mode in the same experiment showed minimal signal (Figure 4G, left panel), suggesting that spatial segregation and/or aggregation is not sufficient to induce Notch activation.

Finally, we investigated whether ligand-mediated conformational changes or nanoscale oligomerization contributed to receptor activation (Gordon et al., 2015). We conjugated the MPNs with native Notch ligands (Dll1) either monovalently or multivalently (Figures S2 and S4) and then repeated the previous experiments at different force modes. Regardless of their valency (mono- or multivalent) or ligand interactions (BG-SNAP or Dll1-Notch), only the cells treated with the

strong-force mode showed strong nuclear fluorescence (Figure 4G). Repeated experiments with multiple cells confirmed these results (Figure 4H). Three cells treated with the strong-force mode showed almost identical mCherry signals (Figure 4H), indicating that neither physical/chemical crosslinking nor ligand-mediated receptor allostery significantly influences the mechanical signaling dose of Notch receptors. We conclude from these experiments that Notch is a true mechanosensitive protein that does not require ligand-mediated allostery, ligand-mediated oligomerization, or spatial concentration for activation.

Spatial and Mechanical Responses of E-Cadherin Adhesion Molecules

To demonstrate the modularity and general applicability of the MPNs, we investigated signaling dynamics of E-cadherin—a key mediator of mechanical signals and adhesion at cell-cell junctions (Lecuit and Yap, 2015). E-cadherin signaling serves versatile roles in development, homeostasis, and remodeling of epithelial tissues and has been implicated in cancer progression (Lecuit and Yap, 2015; van Roy, 2014). E-cadherin-mediated adherens junction formation accompanies dynamic processes that include *trans*- and *cis*-receptor interactions, receptor segregation, mechanical activation, recruitment of junction complex proteins, and interactions with the actin cytoskeleton (Lecuit and Yap, 2015). How receptor spatial organization and mechanical loading cooperate to affect the key steps of adaptor recruitment and actin polymerization has not been explicitly tested in live cells, due to the inability to decouple spatial and mechanical cues.

To visualize F-actin dynamics in response to receptor segregation and mechanical loading of E-cadherin, we co-transfected U2OS cells with plasmids encoding SNAP-Ecad-mEmerald and Lifeact7-mCherry and then labeled them with BG-MPNs. First, we induced spatial localization of the nanoprobes—and, hence, E-cadherin—by placing the magnetic tweezer 2 μm above a target subcellular location (weak-force mode). We observed a concentrated mCherry signals at the target subcellular region (Figure 5A), consistent with the notion that E-cadherin clustering induces recruitment of F-actin at or adjacent to E-cadherin clusters (Biswas et al., 2015; Engl et al., 2014; Lecuit and Yap, 2015).

While E-cadherin clustering was sufficient to induce local F-actin assembly, the structure and dynamics of the assemblies differed under the weak and strong forces. Under the weak-force regime, F-actin assemblies showed a circular shape rather than defined filamentous actin network structure (Figure 5B, top). We also observed rapid relaxation of E-cadherin and F-actin fluorescence to initial levels after removal of the magnetic tweezer (Figures 5B and 5D; Movie S4), suggesting that these assemblies were highly transient and dynamic. In contrast, under a strong-force mode (9 pN, d = 0.7 μm), where E-cadherin receptors were both spatially localized and mechanically activated, the recruited F-actin assemblies exhibited diverse structural patterns (e.g., circle, ring, or irregular) and a filamentous network (Lecuit and Yap, 2015) (Figure 5B, bottom). Additionally, upon removal of the tweezer, a significant portion (>50%) of F-actin fluorescence signal was retained, suggesting enhanced F-actin stability upon spatial and mechanical loading of E-cadherin (Figures 5B, 5D, and 5E, Movie S4). We quantified the stability of F-actin after removal of the tweezer with a threshold-and-segmentation algorithm (Figure 5C). Clear differences in actin fluorescence intensity (Figures 5D and 5E) and fluorescence area (Figures 5F and 5G) were observed when E-cadherin was clustered with and without mechanical loading. These observations support the notion that a force-mediated conformational change stabilizes E-cadherin-cytoskeletal complexes. It has been suggested that vinculin recruitment is essential for the stabilization of these complexes (Lecuit and Yap, 2015; Peng et al., 2010; Wu et al., 2014). Therefore, we immunostained cells after stimulating them with either the strong- or the weak-force mode to visualize vinculin distribution at the targeted area. Strong vinculin fluorescence signal was evident for E-cadherin clusters treated with the strong-force mode, whereas negligible vinculin fluorescence was seen at the clusters under the weak-force mode (Figure 5H).

Temporal and Quantitative Control of Mechanosensitive Receptors

Like chemical or electrical signals, the quantity and dynamics of mechanical signals can influence the magnitude of downstream signaling events. Thus, the capacity to quantitatively deliver time-varying inputs to mechanosensitive receptors provides an additional layer of versatility for interrogation of mechanical signaling in a live-cell context.

To test whether MPNs are also suitable for quantitative and dynamic control of signaling downstream of a mechanosensitive receptor, we activated Notch signaling in the UAS-GAL4 reporter cells via MPNs and monitored kinetic time traces of mCherry fluorescence in targeted cells (Figure 6A). We observed a progressive increase of mCherry fluorescence indicating Notch-activated H2B-mCherry transcription after an induction period (Movie S5). To test whether MPN activation induces consistent transcriptional profiles in activated cells, we repeated the experiment for multiple single cells (Figure 6B) and analyzed the activation onset and the mCherry production rate (Figures 6C and S6) (Sprinzak et al., 2010). We also tested the reproducibility of transcriptional activation of multiple cells in a field of view by using spatially programmed magnetic tweezer movement between multiple target cells (Figure 6D). Across multiple cells, the time traces of mCherry fluorescence intensity showed relatively narrow distributions with respect to the activation onset (t_{on} = 6.1 ± 1.4 hr) and production rate (R_{mC} = 0.74 ± 0.19 relative fluorescence units [RFU]·hr^{-1}) (Figure 6C). These properties suggest that MPNs can serve as a powerful platform for the temporal and quantitative control of cell signaling. To further demonstrate this capability, we randomly chose three cells in a population and stimulated Notch signaling of those cells by the probe at 2-hr time intervals (Figure 6E). Consistent with the sequential pattern of activation, the cells produced mCherry sequentially (Figures 6E and 6F; Movie S6). We also varied the tweezer application duration on target cells in a population from 5 min, 10 min, and 20 min (Figure 6G) and measured the rates of mCherry production on a per-cell basis. The mCherry production rate showed an approximately proportional response to the tweezer application duration (Figures 6H and 6I), supporting the quantitative control of Notch signaling by the MPN.

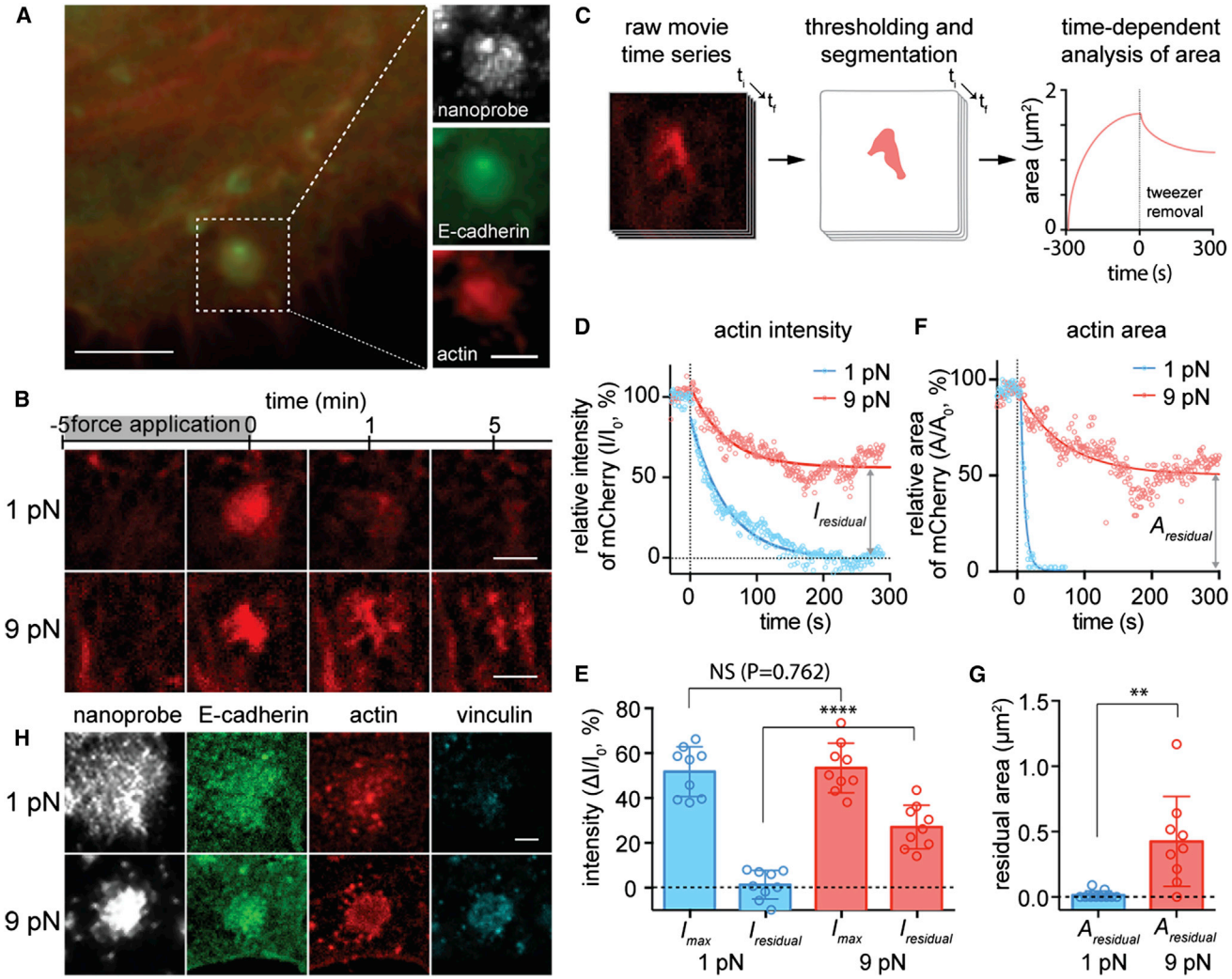

Figure 5. Response of E-Cadherin to Spatial and Mechanical Perturbation with MPNs

(A) Subcellular localization of E-cadherin receptors (green) in U2OS cells by MPNs induces F-actin (red) recruitment. Scale bars, 5 μm and 2 μm (inset). (B–H) Force response of E-cadherin domain formation at the cell membrane. (B) Time series of F-actin fluorescence images before and after force application by MPNs: (top) weak force (1 pN at d = 2.0 μm) or (bottom) strong force (9 pN at d = 0.7 μm). Scale bars, 2 μm. (C) Outline of thresholding and segmentation algorithm used for analysis of actin recruitment and residual area. (D) Representative intensity trajectories of F-actin fluorescence within a 2-μm circle of tweezing area after removal of the weak- or strong-force mode tweezer. (E) Statistical residual intensity analysis of multiple replicates. (F) Representative time trajectories of F-actin area upon tweezer removal after either weak- or strong-force modes. (G) Statistical residual area analysis of multiple replicates. (H) Immunofluorescence staining for vinculin recruitment after weak- or strong-force application. Scale bar, 2 μm. **$p < 0.01$; ****$p < 0.0001$. Error bars indicate SE.

DISCUSSION

MPN Probes Provide Unprecedented Precision and Modularity to Monitor and Perturb Mechanical Signaling

Mechanosensitive membrane proteins that transduce the mechanical properties of extracellular environments into intracellular chemical signals play a central role in multicellular signaling networks (Vogel and Sheetz, 2006). Their activation can involve a number of discrete steps, including receptor-ligand interaction, spatial segregation, receptor clustering, and mechanical force-induced conformational changes, along with the activity of associated enzymes such as proteases and kinases (Kopan and Ilagan, 2009; Louvi and Artavanis-Tsakonas, 2006; Vogel and Sheetz, 2006).

Toward dissecting the mechanism of mechanically activated cell-surface receptors, several methods have been recently reported for the targeted and localized activation of mechanosensitive proteins (Liu et al., 2016; Sniadecki et al., 2007). Our MPNs incorporate a number of additional and powerful features that complement these methods. These features include quantitative mechanical perturbations, the ability to spatially reorganize proteins independent of mechanical loading, modularity in the level of control from single molecule to a pre-concentrated group of molecules, and access to the apical and lateral cell surfaces to

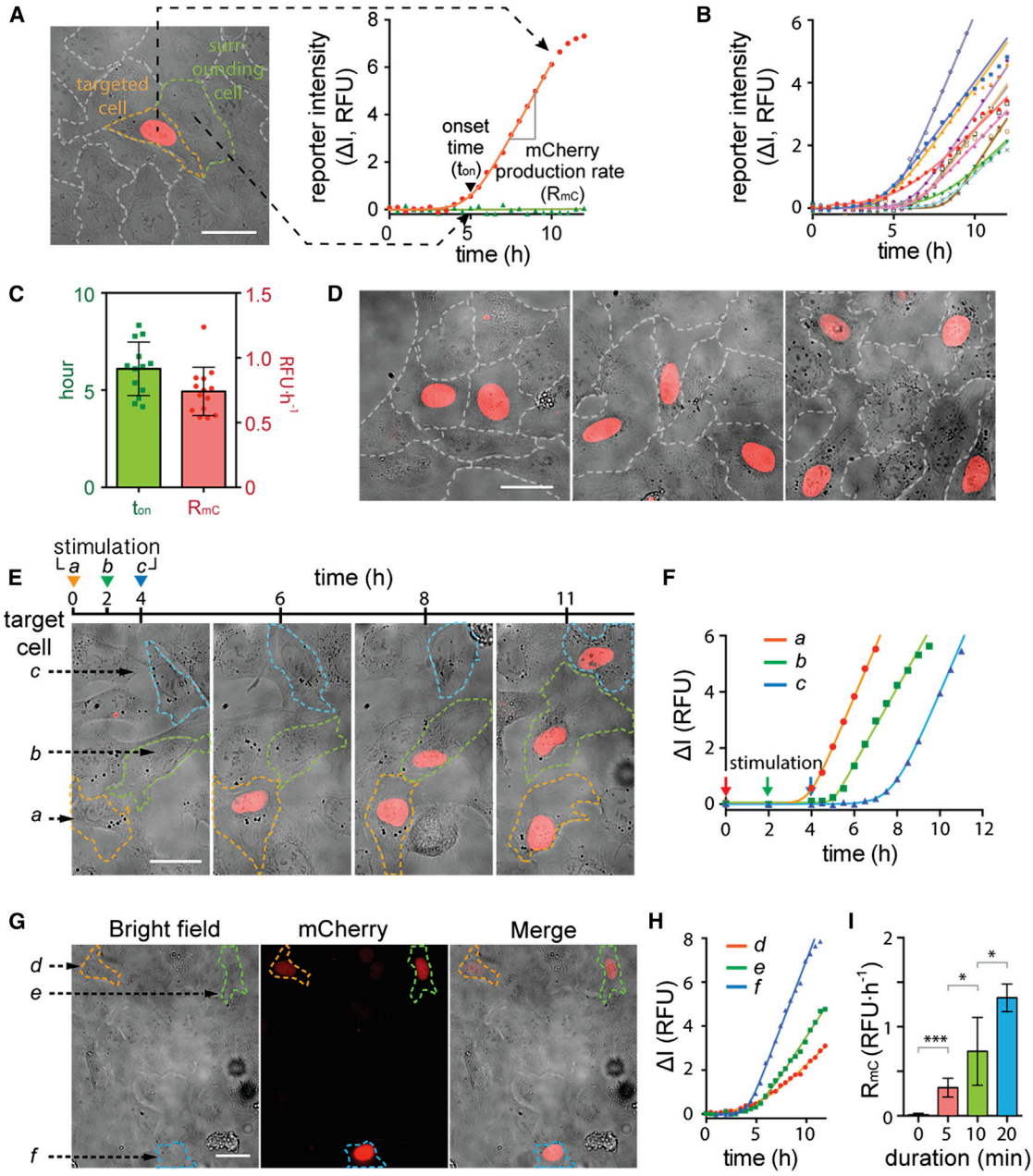

Figure 6. Spatial, Temporal, and Quantitative Control of Gene Transcription after Cell Stimulation with MPNs

(A–C) Single-cell kinetics of H2B-mCherry production in UAS-Gal4 reporter cells after MPN-induced Notch activation. (A) A representative fluorescence image and time trace. (B) Aggregates of multiple cell traces. (C) Statistical analysis of the mCherry production onset (t_{on}) and rate (R_{mC}).

(D) Spatially programmed Notch activation.

(E and F) Temporal control of Notch signaling. (E) Time series images and (F) mCherry fluorescence intensity trajectories of three randomly chosen cells (*a*, *b*, and *c*) in a population after sequential stimulation with time intervals of 2 hr.

(G–I) Quantitative control of cell signaling. (G) Representative images, (H) time traces of the cells, and (I) statistical analysis of the production rate with multiple replicates of three randomly chosen cells in a population after tweezer application in strong-force mode for 5 min (cell d), 10 min (cell e), and 20 min (cell f), respectively.

Scale bars, 30 μm. RFU: relative fluorescence unit. *$p < 0.05$; ***$p < 0.001$. Error bars indicate SE.

simulate sites of cell-cell contact. These capabilities allowed us to identify the differential roles of chemical, spatial, temporal, and mechanical inputs on the activation of two important mechanosensitive receptors: Notch and E-cadherin.

Interrogation of the Activation Mechanism of Notch Receptors

As a first application, we used the MPNs to interrogate the differential role of Notch localization, oligomerization, and mechanical

force on receptor activation with single-cell resolution. Several unique properties of the MPN enabled this application. First, the small size and monovalent character of the nanoprobes facilitated high-density labeling of Notch with one-to-one particle-to-receptor engagement, minimizing probe-induced nonspecific receptor clustering and perturbation of mechanical environment. Hence, Notch receptors were stimulated only if external cues were switched on. Second, the controlled force-generation capability of nanoprobes could induce either spatial segregation of target proteins, facilitating receptor clustering or mechanical activation of target biomolecules. Thus, the differential effects of receptor segregation and mechanical loading could be effectively decoupled by controlling the tweezer mode. For example, we used these unique properties of the MPN to mechanically stimulate Notch in three different contexts: mechanical load only, receptor clustering only, and the combination of these stimuli. Third, the modular functionality of the nanoprobe allowed targeting of Notch by native Notch ligands (e.g., Dll1) or synthetic protein interaction (e.g., BG-SNAP). This allowed us to test the ligand-induced allostery hypothesis while activating single Notch receptors. Fourth, by controlling the valency of nanoparticles (mono- versus multivalent), the role of nanoscale oligomerization on receptor activation could be additionally investigated. Fifth, the high spatial precision of the nanoprobe-micromagnetic tweezer system enables direct comparisons between neighboring cells from a single clonal population exposed to identical environments. Together, these properties of the MPN allowed us to extend a recent report on the mechanosensitivity of Notch using microbeads that showed that ligand-induced conformation changes were not necessary for receptor activation (Gordon et al., 2015). Our study using MPNs additionally shows that mechanical force is necessary and sufficient for Notch activation independent of ligand-induced allosteric changes, receptor oligomerization, and spatial reorganization.

It should be noted that our experiments used a model reporter cell line expressing recombinant Notch receptors with a truncation of the intracellular subdomain responsible for the interaction with transcriptional factors. These constructs were designed to study the early steps in Notch receptor activation. How these spatial (e.g., contact area, clustering states), mechanical, temporal, and biochemical factors (e.g., different ligand systems) contribute to downstream Notch signaling pathways will require future studies (Khait et al., 2016).

Identification of Differential Roles of Spatial Localization and Mechanical Loading in E-Cadherin Signaling

Numerous studies of E-cadherin activation in cell culture have been conducted using substrate- or bead-immobilized E-cadherin, where *trans*-E-cadherin dimers form at the substrate-cell membrane interface, and cellular force exertion to the immobilized E-cadherin dimers activates E-cadherin signaling (Gavard et al., 2004; Ladoux et al., 2010). This approach to studying E-cadherin alters receptor diffusion and oligomerization and thus fails to fully recapitulate the mechanisms underlying E-cadherin junction formation in vivo. SLBs can resolve these issues, and a recent study found that increased membrane viscosity is also critical for E-cadherin nucleation, clustering, and recruitment of junction complex proteins (Biswas et al., 2015). However, the interplay between E-cadherin clustering and mechanical force application during E-cadherin junction formation, adaptor recruitment, and cytoskeletal remodeling has yet to be elucidated.

Using MPNs, we were able to effectively decouple spatial from mechanical cues to dissect the differential roles of spatial localization and mechanical force in activation of E-cadherin junction formation. We found that spatial localization of E-cadherin initiates F-actin assembly at or around the E-cadherin clusters, but mechanical force stabilizes F-actin to form filamentous networks along with recruitment of vinculin, a junction-stabilizing molecule (Engl et al., 2014; Lecuit and Yap, 2015). This result is consistent with recent in vitro observations of force-induced (>5 pN) α-catenin (the mechanosensitive component protein of E-cadherin junctions) unfolding, vinculin recruitment, and enhanced α-catenin/actin interaction under force (>8 pN) (Buckley et al., 2014; Yao et al., 2014), suggesting that a similar force-induced junction stabilization mechanism occurs in live cells. How cluster size, lateral mobility, and the quality of molecular interaction (e.g., *cis*- and *trans*-interactions of E-cadherin) during E-cadherin assembly influence adherens junction dynamics, polarity, and stability is largely unknown (Lecuit and Yap, 2015; Rakshit and Sivasankar, 2014). Coupled with other available imaging and sensing technologies, we believe that the capacity of MPNs to deliver controlled spatial, temporal, chemical, and mechanical cues to live cells will be useful in tackling outstanding questions in these and other mechanosensitive cell signaling systems.

EXPERIMENTAL PROCEDURES

Preparation of Monovalent MPNs: $Zn_{0.4}Fe_{2.6}O_4$@SiO_2@Au

MPNs were synthesized by a sequential growth strategy. First, zinc-doped iron oxide ($Zn_{0.4}Fe_{2.6}O_4$) nanoparticles were synthesized via a literature method (Jang et al., 2009), were coated with amine-functionalized silica, and were further coated with gold shell via literature procedures with modifications (Wang et al., 2007). MPNs were monovalently conjugated with thiolated DNA via Au-thiol chemistry. Experimental conditions and purification methods are detailed in the Supplemental Experimental Procedures.

Calibration of Force Exerting on a Single Particle

Distance-dependent force exertion on a single MPN was determined by either measuring rupture distance of MPN-linked TGT-DNA force sensors with known rupture values or performing a viscous drag force experiment of the nanoparticles in a water-glycerol mixture. Experimental details are described in the Supplemental Experimental Procedures.

SLB Experiments

The bilayers containing nickel-nitrilotriacetic acid (Ni-NTA) functional groups were formed on cover glass and then sequentially incubated with His-tagged SNAP protein, BG-DNA, and monovalent MPNs bearing complementary sequences (Farlow et al., 2013). Experimental details and DNA sequences are described in the Supplemental Experimental Procedures.

Cloning and Protein Expression

SNAP-hN1-mCherry and SNAP-hN1-Gal4 were constructed via traditional cloning methods. U2OS stable cell lines expressing either SNAP-hN1-mCherry or SNAP-hN1-Gal4 proteins were generated by stably incorporating these constructs into a parental U2OS T-rex cell line by the Flp-IN system. SNAP-Ecad-mEmerald was constructed by insertion of the SNAP tag sequence (New England Biolabs) behind the signal and pro-peptide sequences of E-cadherin. Co-transfection of SNAP-Ecad-mEmerald and

LifeAct7-mCherry was performed by electroporation. Experimental details are described in the Supplemental Experimental Procedures.

Live-Cell Experiments

Cells expressing recombinant constructs were cultured and observed on collagen-coated glass-bottom dishes. For labeling cells via BG/SNAP chemistry, cells were sequentially incubated with BG-DNA and MPNs bearing complementary sequences. For force application experiments, the magnetic tweezer was brought toward the target subcellular while the fluorescence response was monitored under epi-fluorescence. Experimental details are described in the Supplemental Experimental Procedures.

Image Processing and Analysis of Fluorescence Signals

Single-cell tracking and nuclear fluorescence signal analysis of cells were performed with ImageJ. mCherry fluorescence intensities of individual cells were measured and corrected by subtracting the background signal with the same pixel area. Custom python code adapted from Gay (2014) was used for image processing and measurement of actin accumulation. Experimental details are described in the Supplemental Experimental Procedures.

SUPPLEMENTAL INFORMATION

Supplemental Information includes Supplemental Experimental Procedures, six figures, and six movies and can be found with this article online at http://dx.doi.org/10.1016/j.cell.2016.04.045.

AUTHOR CONTRIBUTIONS

D.S. and Y.J. conceived and designed the project; D.S., J.K., J.L., J.C., and Y.J. contributed nanoparticle synthesis; D.S., K.M.S., Z.J.G., and Y.J. designed biological experiments; D.S., K.M.S., J.K., J.F., H.J.L., and J.L. performed experiments; D.S. and K.M.S. analyzed and interpreted the data; D.B.L. performed electron microscope analysis; T.H. and A.P.A. provided feedback on the experiment and data interpretation; and D.S., K.M.S., Z.J.G., and Y.J. wrote the manuscript. All authors discussed and commented on the manuscript.

ACKNOWLEDGMENTS

The authors thank S. Blacklow (Harvard University) for the generous gift of Notch plasmids, Y. J. Lim for magnetic nanoparticle synthesis, and the Marvell Nanofabrication Laboratory for use of electron microscope facilities. This work was supported by grant 1R01GM112081-01 from the National Institute of General Medical Science (NIGMS) (Y.J.), a UCSF/UCB/LBNL BRAINseed award (Y.J.), grant 1R21EB015088-01 from the National Institute of Biomedical Imaging and Bioengineering (Z.J.G. and Y.J.), grant DP2 HD080351-01 from the National Institute of Child Health and Human Development (Z.J.G.), grant P50 GM081879 from the NIGMS UCSF Center for Synthetic and Systems Biology (Z.J.G.), a Human Frontier Science Program Fellowship (D.S.), grant IBS-R026-D1 from IBS (J.C. and Y.J.), grant 2010-0018286 from the National Creative Research Initiatives Program (J.C.), grant HI08C2149 from the Korea Healthcare Technology R&D Project (J.C.), and a grant from King Abdulaziz City for Science and Technology (A.P.A.).

Received: June 19, 2015
Revised: February 17, 2016
Accepted: April 13, 2016
Published: May 12, 2016

REFERENCES

Banghart, M., Borges, K., Isacoff, E., Trauner, D., and Kramer, R.H. (2004). Light-activated ion channels for remote control of neuronal firing. Nat. Neurosci. *7*, 1381–1386.

Bharde, A.A., Palankar, R., Fritsch, C., Klaver, A., Kanger, J.S., Jovin, T.M., and Arndt-Jovin, D.J. (2013). Magnetic nanoparticles as mediators of ligand-free activation of EGFR signaling. PLoS ONE *8*, e68879.

Biswas, K.H., Hartman, K.L., Yu, C.-H., Harrison, O.J., Song, H., Smith, A.W., Huang, W.Y.C., Lin, W.-C., Guo, Z., Padmanabhan, A., et al. (2015). E-cadherin junction formation involves an active kinetic nucleation process. Proc. Natl. Acad. Sci. USA *112*, 10932–10937.

Buckley, C.D., Tan, J., Anderson, K.L., Hanein, D., Volkmann, N., Weis, W.I., Nelson, W.J., and Dunn, A.R. (2014). Cell adhesion. The minimal cadherin-catenin complex binds to actin filaments under force. Science *346*, 1254211.

Cho, M.H., Lee, E.J., Son, M., Lee, J.-H., Yoo, D., Kim, J.-W., Park, S.W., Shin, J.-S., and Cheon, J. (2012). A magnetic switch for the control of cell death signalling in in vitro and in vivo systems. Nat. Mater. *11*, 1038–1043.

Cocco, S., Monasson, R., and Marko, J.F. (2001). Force and kinetic barriers to unzipping of the DNA double helix. Proc. Natl. Acad. Sci. USA *98*, 8608–8613.

Deisseroth, K. (2011). Optogenetics. Nat. Methods *8*, 26–29.

Dufrêne, Y.F., Evans, E., Engel, A., Helenius, J., Gaub, H.E., and Müller, D.J. (2011). Five challenges to bringing single-molecule force spectroscopy into living cells. Nat. Methods *8*, 123–127.

Engl, W., Arasi, B., Yap, L.L., Thiery, J.P., and Viasnoff, V. (2014). Actin dynamics modulate mechanosensitive immobilization of E-cadherin at adherens junctions. Nat. Cell Biol. *16*, 587–594.

Etoc, F., Lisse, D., Bellaiche, Y., Piehler, J., Coppey, M., and Dahan, M. (2013). Subcellular control of Rac-GTPase signalling by magnetogenetic manipulation inside living cells. Nat. Nanotechnol. *8*, 193–198.

Farlow, J., Seo, D., Broaders, K.E., Taylor, M.J., Gartner, Z.J., and Jun, Y.-W. (2013). Formation of targeted monovalent quantum dots by steric exclusion. Nat. Methods *10*, 1203–1205.

Gavard, J., Lambert, M., Grosheva, I., Marthiens, V., Irinopoulou, T., Riou, J.-F., Bershadsky, A., and Mège, R.-M. (2004). Lamellipodium extension and cadherin adhesion: two cell responses to cadherin activation relying on distinct signalling pathways. J. Cell Sci. *117*, 257–270.

Gay, G. (2014). Segmenting nuclei with skimage. http://damcb.com/segmenting-nuclei.html.

Gordon, W.R., Vardar-Ulu, D., Histen, G., Sanchez-Irizarry, C., Aster, J.C., and Blacklow, S.C. (2007). Structural basis for autoinhibition of Notch. Nat. Struct. Mol. Biol. *14*, 295–300.

Gordon, W.R., Zimmerman, B., He, L., Miles, L.J., Huang, J., Tiyanont, K., McArthur, D.G., Aster, J.C., Perrimon, N., Loparo, J.J., and Blacklow, S.C. (2015). Mechanical allostery: evidence for a force requirement in the proteolytic activation of Notch. Dev. Cell *33*, 729–736.

Ho, D., Zimmermann, J.L., Dehmelt, F.A., Steinbach, U., Erdmann, M., Severin, P., Falter, K., and Gaub, H.E. (2009). Force-driven separation of short double-stranded DNA. Biophys. J. *97*, 3158–3167.

Hoffmann, C., Mazari, E., Lallet, S., Le Borgne, R., Marchi, V., Gosse, C., and Gueroui, Z. (2013). Spatiotemporal control of microtubule nucleation and assembly using magnetic nanoparticles. Nat. Nanotechnol. *8*, 199–205.

Iskratsch, T., Wolfenson, H., and Sheetz, M.P. (2014). Appreciating force and shape—the rise of mechanotransduction in cell biology. Nat. Rev. Mol. Cell Biol. *15*, 825–833.

Jang, J.-T., Nah, H., Lee, J.-H., Moon, S.H., Kim, M.G., and Cheon, J. (2009). Critical enhancements of MRI contrast and hyperthermic effects by dopant-controlled magnetic nanoparticles. Angew. Chem. Int. Ed. Engl. *48*, 1234–1238.

Khait, I., Orsher, Y., Golan, O., Binshtok, U., Gordon-Bar, N., Amir-Zilberstein, L., and Sprinzak, D. (2016). Quantitative analysis of Delta-like 1 membrane dynamics elucidates the role of contact geometry on Notch signaling. Cell Rep. *14*, 225–233.

Kopan, R., and Ilagan, M.X.G. (2009). The canonical Notch signaling pathway: unfolding the activation mechanism. Cell *137*, 216–233.

Ladoux, B., Anon, E., Lambert, M., Rabodzey, A., Hersen, P., Buguin, A., Silberzan, P., and Mège, R.-M. (2010). Strength dependence of cadherin-mediated adhesions. Biophys. J. *98*, 534–542.

Lecuit, T., and Yap, A.S. (2015). E-cadherin junctions as active mechanical integrators in tissue dynamics. Nat. Cell Biol. *17*, 533–539.

Levskaya, A., Weiner, O.D., Lim, W.A., and Voigt, C.A. (2009). Spatiotemporal control of cell signalling using a light-switchable protein interaction. Nature *461*, 997–1001.

Liu, Z., Liu, Y., Chang, Y., Seyf, H.R., Henry, A., Mattheyses, A.L., Yehl, K., Zhang, Y., Huang, Z., and Salaita, K. (2016). Nanoscale optomechanical actuators for controlling mechanotransduction in living cells. Nat. Methods *13*, 143–146.

Louvi, A., and Artavanis-Tsakonas, S. (2006). Notch signalling in vertebrate neural development. Nat. Rev. Neurosci. *7*, 93–102.

Mannix, R.J., Kumar, S., Cassiola, F., Montoya-Zavala, M., Feinstein, E., Prentiss, M., and Ingber, D.E. (2008). Nanomagnetic actuation of receptor-mediated signal transduction. Nat. Nanotechnol. *3*, 36–40.

Miesenböck, G. (2009). The optogenetic catechism. Science *326*, 395–399.

Mosayebi, M., Louis, A.A., Doye, J.P.K., and Ouldridge, T.E. (2015). Force-induced rupture of a DNA duplex: from fundamentals to force sensors. ACS Nano *9*, 11993–12003.

Neuman, K.C., and Nagy, A. (2008). Single-molecule force spectroscopy: optical tweezers, magnetic tweezers and atomic force microscopy. Nat. Methods *5*, 491–505.

Peng, X., Cuff, L.E., Lawton, C.D., and DeMali, K.A. (2010). Vinculin regulates cell-surface E-cadherin expression by binding to beta-catenin. J. Cell Sci. *123*, 567–577.

Rakshit, S., and Sivasankar, S. (2014). Biomechanics of cell adhesion: how force regulates the lifetime of adhesive bonds at the single molecule level. Phys. Chem. Chem. Phys. *16*, 2211–2223.

Sniadecki, N.J., Anguelouch, A., Yang, M.T., Lamb, C.M., Liu, Z., Kirschner, S.B., Liu, Y., Reich, D.H., and Chen, C.S. (2007). Magnetic microposts as an approach to apply forces to living cells. Proc. Natl. Acad. Sci. USA *104*, 14553–14558.

Sprinzak, D., Lakhanpal, A., Lebon, L., Santat, L.A., Fontes, M.E., Anderson, G.A., Garcia-Ojalvo, J., and Elowitz, M.B. (2010). Cis-interactions between Notch and Delta generate mutually exclusive signalling states. Nature *465*, 86–90.

Stephenson, N.L., and Avis, J.M. (2012). Direct observation of proteolytic cleavage at the S2 site upon forced unfolding of the Notch negative regulatory region. Proc. Natl. Acad. Sci. USA *109*, E2757–E2765.

Toettcher, J.E., Voigt, C.A., Weiner, O.D., and Lim, W.A. (2011). The promise of optogenetics in cell biology: interrogating molecular circuits in space and time. Nat. Methods *8*, 35–38.

Tseng, P., Judy, J.W., and Di Carlo, D. (2012). Magnetic nanoparticle-mediated massively parallel mechanical modulation of single-cell behavior. Nat. Methods *9*, 1113–1119.

van Roy, F. (2014). Beyond E-cadherin: roles of other cadherin superfamily members in cancer. Nat. Rev. Cancer *14*, 121–134.

Vogel, V., and Sheetz, M. (2006). Local force and geometry sensing regulate cell functions. Nat. Rev. Mol. Cell Biol. *7*, 265–275.

Wang, X., and Ha, T. (2013). Defining single molecular forces required to activate integrin and notch signaling. Science *340*, 991–994.

Wang, H., Brandl, D.W., Nordlander, P., and Halas, N.J. (2007). Plasmonic nanostructures: artificial molecules. Acc. Chem. Res. *40*, 53–62.

Weber, R.J., Liang, S.I., Selden, N.S., Desai, T.A., and Gartner, Z.G. (2014). Efficient targeting of fatty-acid modified oligonucleotides to live cell membranes through stepwise assembly. Biomacromolecules *15*, 4621–4626.

Wu, S.K., Gomez, G.A., Michael, M., Verma, S., Cox, H.L., Lefevre, J.G., Parton, R.G., Hamilton, N.A., Neufeld, Z., and Yap, A.S. (2014). Cortical F-actin stabilization generates apical-lateral patterns of junctional contractility that integrate cells into epithelia. Nat. Cell Biol. *16*, 167–178.

Yao, M., Qiu, W., Liu, R., Efremov, A.K., Cong, P., Seddiki, R., Payre, M., Lim, C.T., Ladoux, B., Mège, R.-M., and Yan, J. (2014). Force-dependent conformational switch of α-catenin controls vinculin binding. Nat. Commun. *5*, 4525.